JGR Oceans

RESEARCH ARTICLE
10.1029/2019JC015516

Decomposing Barotropic Transport Variability in a High-Resolution Model of the North Atlantic Ocean

Yuan Wang[1,2], Richard J. Greatbatch[2,3], Martin Claus[2,3], and Jinyu Sheng[1]

[1]Department of Oceanography, Dalhousie University, Halifax, Nova Scotia, Canada, [2]GEOMAR Helmholtz Centre for Ocean Research Kiel, Kiel, Germany, [3]Faculty of Mathematics and Natural Sciences, University of Kiel, Kiel, Germany

Key Points:

- A linear shallow water model is shown to be an effective means of decomposing the barotropic transport variability in a high-resolution, eddying model of the North Atlantic based on the vertically averaged horizontal momentum equations
- In the model, the mean flow advection and eddy momentum flux terms play an important role in the dynamics of the variability of the barotropic transport of the Gulf Stream and its recirculation gyres
- The mean flow advection and eddy momentum flux contributions sometimes obscure the transport variability associated with the density field

Correspondence to:
R. J. Greatbatch,
rgreatbatch@geomar.de

Citation:
Wang, Y., Greatbatch, R. J., Claus, M., & Sheng, J. (2020). Decomposing barotropic transport variability in a high-resolution model of the North Atlantic Ocean. *Journal of Geophysical Research: Oceans*, *124*. https://doi.org/10.1029/2019JC015516

Received 22 JUL 2019
Accepted 12 MAR 2020
Accepted article online 16 MAR 2020

Abstract A method using a linear shallow water model is presented for decomposing the temporal variability of the barotropic stream function in a high-resolution ocean model. The method is based on the vertically averaged momentum equations and is applied to the time series of annual mean stream function from the model configuration VIKING20 for the northern North Atlantic. An important result is the role played by the nonlinear advection terms in VIKING20 for driving transport. The method is illustrated by examining how the Gulf Stream transport in the recirculation region responds to the winter North Atlantic Oscillation (NAO). While no statistically significant response is found in the year overlapping with the winter NAO index, there is a tendency for the Gulf Stream transport to increase as the NAO becomes more positive. This becomes significant in lead years 1 and 2 when the mean flow advection and eddy momentum flux contributions, associated with nonlinear momentum advection, dominate. Only after 2 years, does the potential energy term, associated with the density field, start to play a role and it is only after 5 years that the transport dependence on the NAO ceases to be significant. It is also shown that the potential energy contribution to the transport stream function has significant memory of up to 5 years in the Labrador and Irminger Seas. However, it is only around the northern rim of these seas that VIKING20 and the transport reconstruction exhibit similar memory. This is due to masking by the mean flow advection and eddy momentum flux contributions.

Plain Language Summary The Gulf Stream plays an important role in the climate system, redistributing heat and other tracers, including carbon, between the tropics and higher latitudes. How the transport of the Gulf Stream varies, in particular in response to forcing from the atmosphere, is still not fully understood. Here we use a novel decomposition technique to identify the different contributions to the transport variability in a high-resolution model configuration for the northern North Atlantic. We find an important role for the nonlinear terms in the momentum balance. Transport variations associated with these terms are often not taken account of but can sometimes obscure signals that are present in the density field.

1. Introduction

There is evidence of significant interannual to decadal variability in the circulation of the North Atlantic Ocean (e.g., DiNezio et al., 2009; Eden & Jung, 2001; Eden & Willebrand, 2001; Greatbatch et al., 1991; Joyce et al., 2000; McCarthy et al., 2018; Rossby et al., 2010; Smeed et al., 2018). Here we focus on the variability of the vertically integrated (barotropic) transport. Understanding what contributes to this transport variability is a topic of ongoing research. High-resolution ocean models offer a tool for making headway but unraveling the different processes that drive transport poses a challenge.

In the present study, we investigate the vertically integrated (barotropic) transport variability in a high-resolution model of the North Atlantic. Such variability can be understood in terms of the vorticity equation derived from either the vertically integrated or the vertically averaged momentum equations (e.g., Bell, 1999; Yeager, 2015). Using the diagnostic model of Mellor et al. (1982), Greatbatch et al. (1991) exploited both approaches and suggested a decomposition based on the linear momentum/vorticity balance. Much less work has been done on the role played by the nonlinear advection terms in the momentum equations. Using an approach based on integrating a linear shallow water model (SWM) to steady state, with the eddy momentum flux (EMF) specified based on satellite data, Greatbatch et al. (2010) suggested an important role for the EMF terms in driving mean transport in the Gulf Stream extension region. The same

methodology was later extended by Wang et al. (2017) to study the dynamics of the mean barotropic transport stream function, where the primary forcing terms for a linear SWM, based on the vertically averaged momentum equations, were diagnosed from a high-resolution ocean model configuration of the North Atlantic, VIKING20 (Behrens, 2013; Böning et al., 2016). These forcing terms are the potential energy (PE) term (which leads to the JEBAR term in the vorticity equation) associated with the density field, the mean flow advection (MFA), and EMF terms that arise from the nonlinear advection terms in the momentum equations carried by VIKING20, and the wind stress (WS) term, in this case the effect of the surface WS applied to a uniform density ocean.

Here the methodology of Wang et al. (2017) is used to decompose the temporal variability in the same high-resolution ocean model of the North Atlantic into the four transport components. The decomposition is then illustrated by using it to interpret the response of the transport to the winter North Atlantic Oscillation (NAO). The NAO is the dominant mode of low-frequency variability in the atmospheric circulation over the North Atlantic (Greatbatch, 2000; Hurrell et al., 2003; Marshall et al., 2001). The Gulf Stream is suggested to vary in transport by up to 8 Sv in response to the NAO and move north (south) in the positive (negative) NAO phase with a shift in order of 10 km (e.g., De Coëtlogon et al., 2006; Joyce & Zhang, 2010; Taylor & Stephens, 1998; Watelet et al., 2017). Rossby et al. (2010) also note a significant (negative) correlation between transport near 55-m depth and the NAO along the "Oleander" line crossing the Gulf Stream near 70°W. In the subpolar gyre, the lateral transport is thought to play a role in climate variability (e.g., Delworth et al., 1993), and the thermohaline forcing exhibits a close relationship to the NAO index (Curry & McCartney, 2001; Dickson et al., 1996; Yashayaev, 2007). In addition, the convectively formed water masses are estimated to have a residence time of approximately 4–5 years in the Labrador basin (Straneo et al., 2003) and to arrive in the Irminger and Iceland basins with typical delays up to 5 years (Yashayaev, 2007). To what extent the spreading of newly formed dense water influences the barotropic transport variability is not clear, although Gerdes and Köberle (1995) offer a glimpse of what can happen in a model that does not resolve eddies.

Another important point to note when interpreting our results is that because our focus is on interannual time scales, classical (flat-bottomed) Sverdrup balance is unlikely to be valid because of the much longer time scales required for baroclinic adjustment of the ocean (e.g., Anderson and Killworth, 1977; Anderson et al., 1979; DiNezio et al., 2009; see also Anderson and Corry (1985) for an illustration on seasonal time scales). Rather, as pointed out by these authors, the variable ocean bottom topography plays an important role. Indeed, Eden and Willebrand (2001) note that the response of the North Atlantic within the first year to forcing from the NAO is expected to be the topographic Sverdrup response to the NAO-induced wind forcing, consistent with what we present here from VIKING20.

The plan of our paper is as follows. The data and methods are described in section 2, the results are presented in section 3, and a summary is provided in section 4.

2. Data and Methods

To compute the annual-mean barotropic transport driven by each of the four forcing terms, the linear, barotropic SWM described in Wang et al. (2017) is run to steady state for each year and each forcing term separately. The SWM uses a staggered latitude/longitude C-grid with a horizontal resolution of 1/20° covering the North Atlantic between 85°W and 5°E and from 31 to 67°N, with the lateral boundaries closed. In steady state, the equations governing the SWM are

$$-fv = Z - \frac{1}{\rho_0 a\cos\theta}\frac{\partial p_b}{\partial \lambda} - \frac{ru}{H} - F_x \tag{1}$$

$$fu = M - \frac{1}{\rho_0 a}\frac{\partial p_b}{\partial \theta} - \frac{rv}{H} - F_y \tag{2}$$

$$0 = \frac{1}{a\cos\theta}\left[\frac{\partial Hu}{\partial \lambda} + \frac{\partial \cos\theta Hv}{\partial \theta}\right] \tag{3}$$

where each of the four forcing terms are denoted as (Z,M), a is the radius of the Earth, and (λ, θ) are

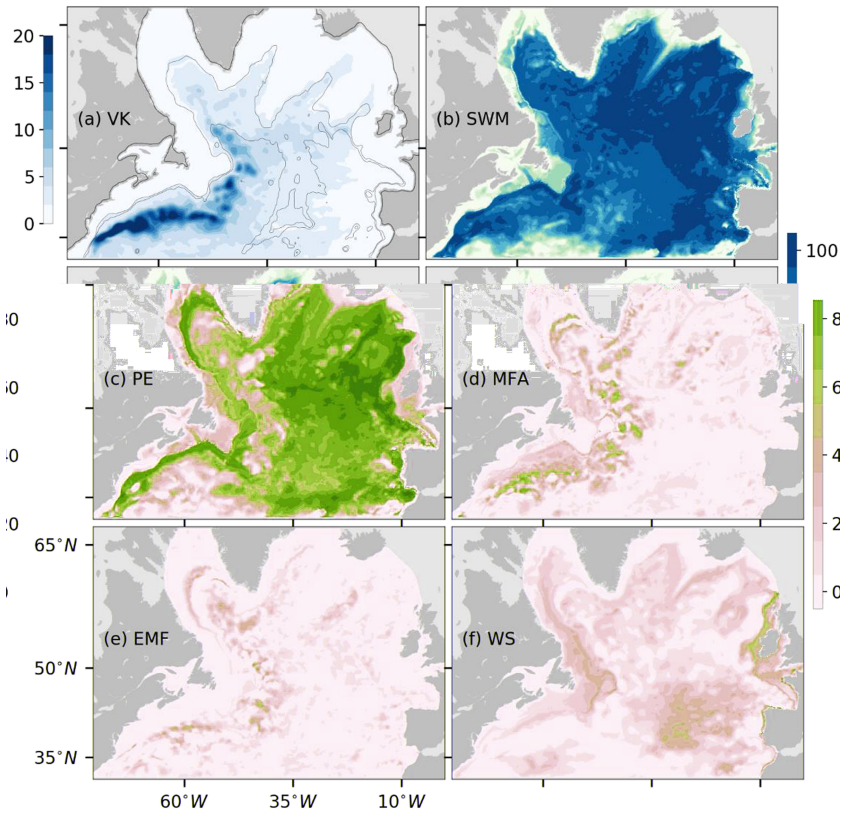

Figure 1. (a) Standard deviation of the annual mean barotropic transport stream function (color image in units of Sverdrups) from VIKING20 (VK), and the percentage of variance in VIKING20 accounted for by (b) the shallow water model (SWM) reconstruction, (c) the potential energy (PE), (d) the mean flow advection (MFA), (e) the eddy momentum flux (EMF), and (f) the wind stress (WS) contributions. Here explained variance is computed using equation (4).

longitude and latitude. It should be noted that the free surface variable in the SWM should be interpreted as the bottom pressure, p_b; ρ_0 is a representative density for sea water; u and v are vertically averaged velocities in the eastward and northward directions, respectively; H is the ocean depth; r is a linear friction coefficient, and (F_x, F_y) denotes a horizontal Laplacian viscosity term with lateral eddy viscosity coefficient A_h (see Wang et al., 2017, for the details). It should be noted that (3) allows the computation of a transport stream function from the SWM output and that a transport stream function is also computed using annual mean output from VIKING20 (see below).

The forcing terms, (Z, M), in equations (1) and (2) are computed from VIKING20 (Behrens, 2013). VIKING20 is a high-resolution (1/20°) configuration, covering the northern North Atlantic Ocean (~30–85°N), nested within a global ocean-ice model of roughly 1/4° horizontal resolution (the base model). The model uses the Nucleus for European Modelling of the Ocean (Madec, 2008), the Louvain-la-Neuve Ice Model (LIM2) model, and two-way nesting using the AGRIF system (see Behrens, 2013, and Böning et al., 2016, for details). After a 30-year spin-up with the base model alone, VIKING20 was integrated from 1948 to 2009 using the interannually varying COREII atmospheric forcing (Large & Yeager, 2009). Output from VIKING20 covering the 50-year period 1960–2009 is used here. The forcing terms (Z, M) are calculated using the output, which consists of 5-day means, for each year separately (see Wang et al., 2017 for details).

The formulation of (Z, M) in the four cases is given below, where an overbar denotes a time average over a single year (following Rieck et al., 2015), prime deviations from that average, and $< >$ a vertical integral from $z = -H$ (the ocean bottom) to $z = 0$ (the ocean surface):

1. The PE term:

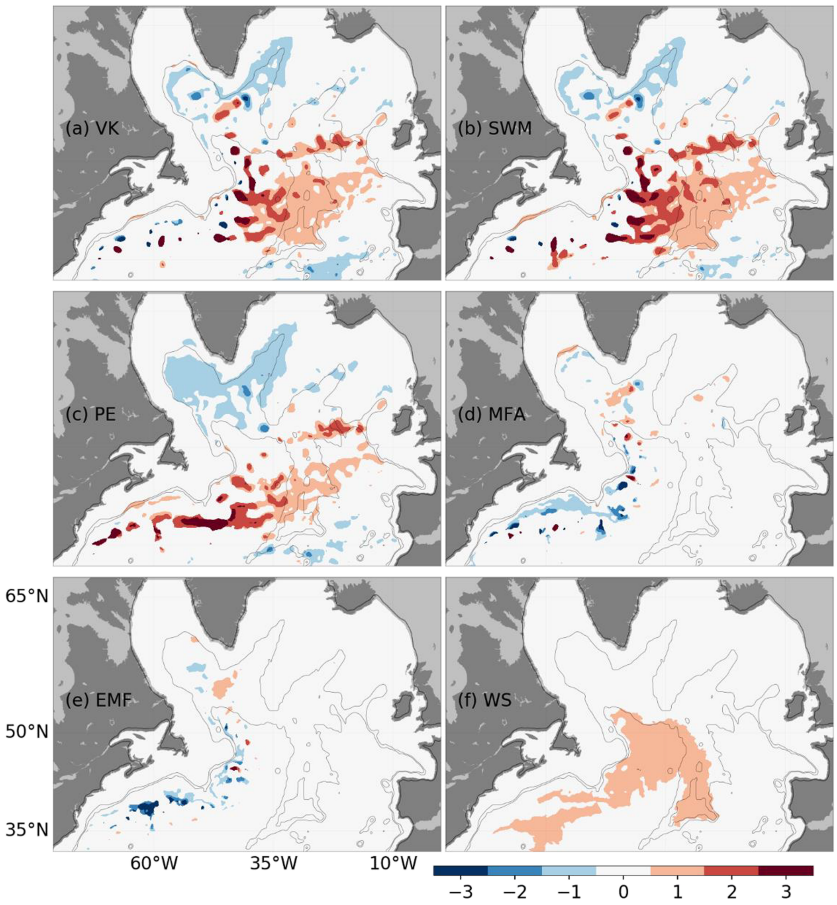

Figure 2. The dependence of the transport stream function on the winter North Atlantic Oscillation (NAO) index as obtained using linear regression for (a) VIKING20 (VK), (b) the shallow water model (SWM), (c) potential energy (PE), (d) mean flow advection (MFA), (e) eddy momentum flux (EMF), and (f) wind stress (WS) contributions. The units are Sv per unit for the NAO index. Only those regions are plotted where the associated correlation exceeds the 95% significance level according to a Student's *t* test.

$$Z = -\frac{1}{Ha\cos\theta}\left[\frac{\partial}{\partial\lambda}\left\langle\frac{\overline{g(\rho-\rho_m)}}{\rho_0}z\right\rangle\right] \qquad M = -\frac{1}{Ha}\left[\frac{\partial}{\partial\theta}\left\langle\frac{\overline{g(\rho-\rho_m)}}{\rho_0}z\right\rangle\right]$$

where ρ represents the in situ density and ρ_m represents the horizontally averaged mean density.

2. The MFA term:

$$Z = -\frac{1}{Ha\cos\theta}\left[\frac{\partial\langle\overline{u}\,\overline{u}\rangle}{\partial\lambda} + \frac{\partial\cos\theta\langle\overline{u}\,\overline{v}\rangle}{\partial\theta}\right] \quad M = -\frac{1}{Ha\cos\theta}\left[\frac{\partial\langle\overline{v}\,\overline{u}\rangle}{\partial\lambda} + \frac{\partial\cos\theta\langle\overline{v}\,\overline{v}\rangle}{\partial\theta}\right]$$

3. The EMF term:

$$Z = -\frac{1}{Ha\cos\theta}\left[\frac{\partial\left\langle\overline{u'u'}\right\rangle}{\partial\lambda} + \frac{\partial\cos\theta\left\langle\overline{u'v'}\right\rangle}{\partial\theta}\right] \quad M = -\frac{1}{Ha\cos\theta}\left[\frac{\partial\left\langle\overline{u'v'}\right\rangle}{\partial\lambda} + \frac{\partial\cos\theta\left\langle\overline{v'v'}\right\rangle}{\partial\theta}\right]$$

4. The WS term

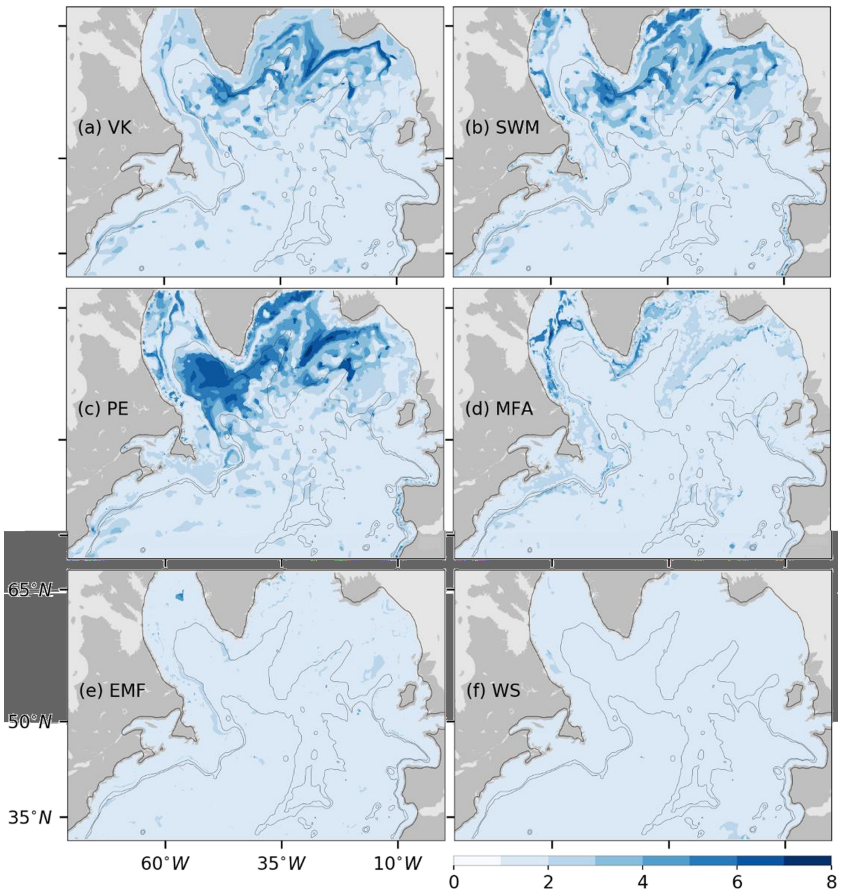

Figure 3. The time in years for the autocorrelation of the transport stream function to drop to a value of 1/e or less in (a) VIKING20 (VK), (b) the shallow water model (SWM) reconstruction, and for the stream function driven by each of (c) the potential energy (PE), (d) mean flow advection (MFA), (e) eddy momentum flux (EMF), and (f) wind stress (WS) terms.

$$Z = \frac{\overline{\tau_s^x}}{\rho_0 H} \qquad M = \frac{\overline{\tau_s^y}}{\rho_0 H}$$

where (τ_s^x, τ_s^y) is the surface WS. Note that to compute terms 2 and 3, VIKING20 does not output the momentum fluxes directly. Rather the 5-day mean output of u and v is used to compute these terms.

When considering the forcing terms 1–4, it should be noted that in the vorticity equation that can be derived from equations (1) to (3), the PE term appears as the JEBAR term (Greatbatch et al., 1991; Mertz & Wright, 1992). Also, the MFA and EMF terms both arise from the nonlinear advection terms in the momentum equations carried by VIKING20, and since the overbar corresponds to an annual mean, the MFA term includes the interannual variability, whereas the EMF term takes account of variability on intraseasonal to seasonal time scales.

In the following, when referring to the SWM reconstruction, we refer to the sum, for each year, of the transport stream functions computed using each forcing term separately.

It should be noted that since the f/H contours enter the model domain at the southern boundary, there is transport that is driven by each of the forcing terms outside the SWM domain that is not accounted for by our model solution. We shall see that for the variability, the role of this "residual part" is not as important as was found for the mean circulation by Wang et al. (2017).

The winter NAO index used in this study is the December–March (DJFM) North Atlantic Oscillation Index (PC-Based; Hurrell, 1995) and was downloaded from https://climatedataguide.ucar.edu. It should be noted that for the analysis in the following sections, the time series have all been detrended.

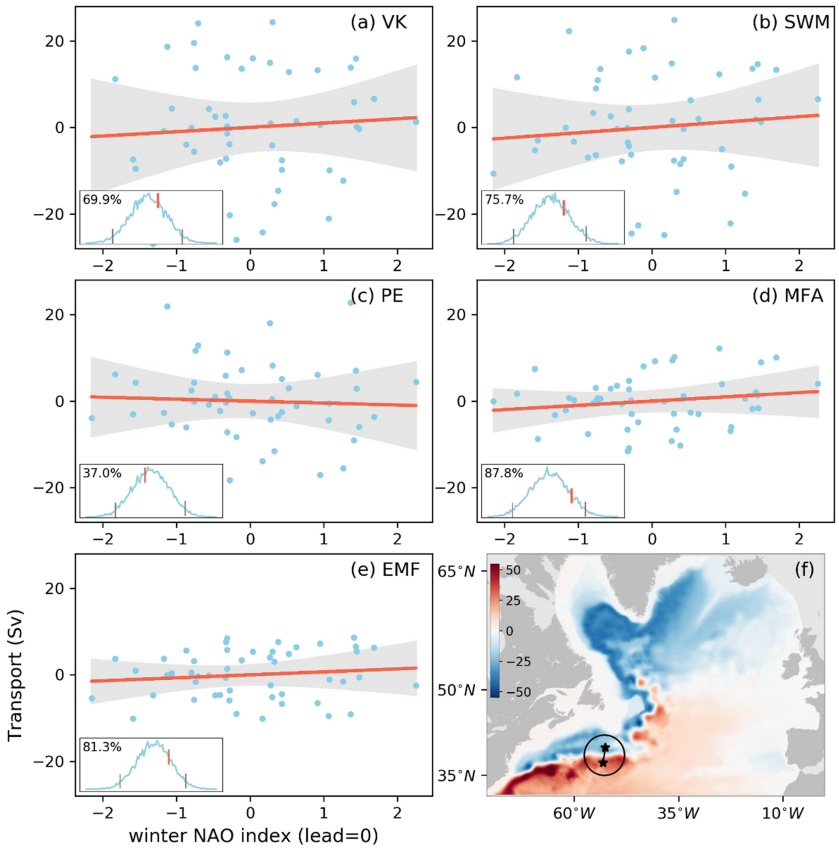

Figure 4. Scatterplot showing, for each year, the winter North Atlantic Oscillation (NAO) index and barotropic transport between the two positions marked by stars shown in (f) for (a) VIKING20 (VK), (b) the shallow water model (SWM) reconstruction and the contributions from (c) the potential energy (PE), (d) mean flow advection (MFA), and (e) eddy momentum flux (EMF) terms. Here the year and winter used for the NAO index overlap in January, February, and March. The time-mean stream function from VIKING20 (color shading) is shown in (f). The red lines are the best fits obtained by the linear regression with the 95% confidence interval shaded in gray (see text for details). The lower left subpanel shows the histogram of the distribution of linear regression slopes obtained by randomly reshuffling the transports, with the 95% significance level indicated by the gray lines (see text for details). The percentages shown on the histogram plots indicate the percentage of linear regression slopes from the Monte Carlo method that are less than the slope of the red line.

3. Results

Figure 1a shows the standard deviation of the annual mean barotropic transport stream function in VIKING20 for the 50-year analysis period, 1960–2009. Over most of the domain, the standard deviation is less than 10 Sv, while somewhat larger (>20 Sv) variability is seen along the pathway of the Gulf Stream and the North Atlantic Current extending into the northwest corner region (Lazier, 1994). As noted by Wang et al. (2017; see also Drews et al., 2015), reproducing the northwest corner is a challenge for most models. In VIKING20, the northwest corner is present but also extends too far northward into the Labrador Sea (see Breckenfelder et al., 2017]).

To compare with the SWM reconstruction, we compute the percentage of variance of the stream function variability in VIKING20 that can be accounted for by the SWM reconstruction as well as the time series of annual mean stream function associated with the different forcing terms. Here explained variance P at each grid point is calculated as

$$P = \left(1 - \frac{\mathrm{var}(\psi_{vk} - \psi)}{\mathrm{var}(\psi_{vk})}\right) \times 100 \tag{4}$$

where ψ_{vk} is the time series of the annual mean stream function from VIKING20, $\mathrm{var}(\psi_{vk})$ is the variance of ψ_{vk}, and ψ is a time series of an annual mean stream function computed using the SWM. It should be noted

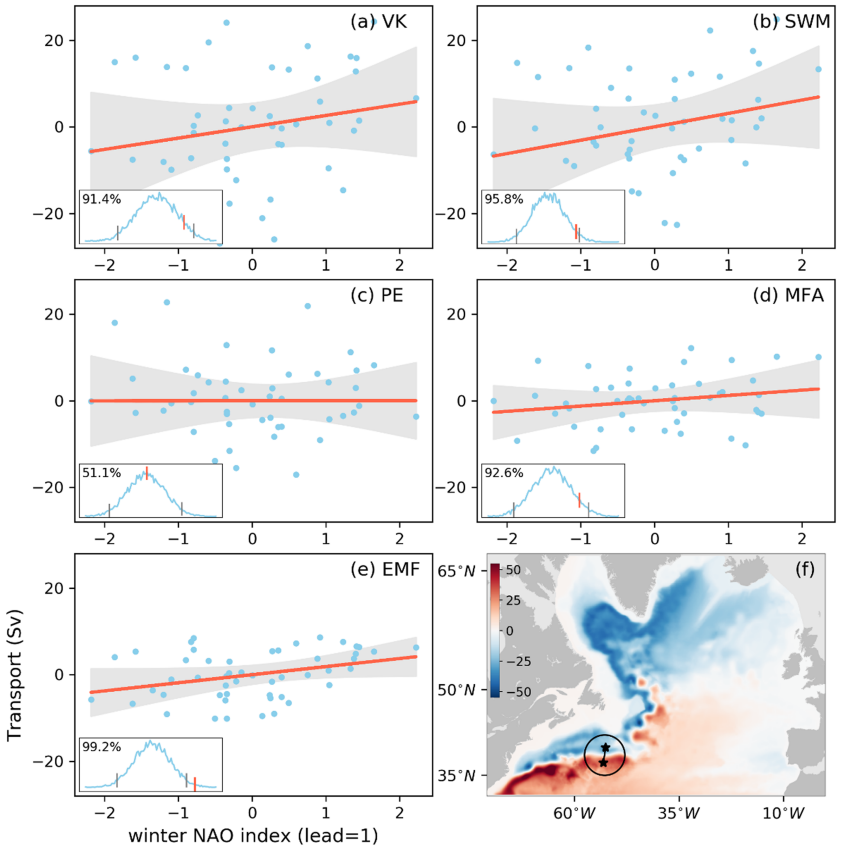

Figure 5. (a–f) As the Figure 4 but for the barotropic transport 1 year later (lead year 1).

that in all cases, the results are almost the same if the explained variance is computed as the square of the linear correlation coefficient between the times series of the two annual mean stream functions.

Figure 1b shows the spatial distribution of *P* computed using the SWM reconstruction, that is, the sum of the stream functions computed separately using the four forcing terms. It is clear that the SWM reconstruction accounts for a large part of the variance seen in VIKING20. Exceptions are near the southern boundary and in the continental shelf regions. The latter is because the bottom topography used for the SWM differs from that in VIKING20 on the shelf. As explained by Wang et al. (2017), this was done for numerical reasons. The discrepancy near the southern boundary is because the SWM does not account for stream function variations that are generated south of the model domain and that propagate into the domain along f/H contours.

The other panels in Figure 1 show the percent variance of the temporal variability in VIKING20 that is explained by stream function variability driven by each of the forcing terms used to drive the SWM. It is clear that most of the variance is explained by the PE case, although there are regions, particularly on the western side of the basin, where other contributions, especially from the MFA and to some extent the EMF cases, play a more important role. This is especially true in the region of the Gulf Stream and associated recirculation gyres south of Atlantic Canada and also in the Labrador Sea.

The WS case (Figure 1f) generally plays only a minor role. To understand why this is, it should be remembered that WS corresponds to the transport stream function variability for the wind-driven response of the ocean as if it had uniform density. Even in the mean, the transport for a uniform density ocean is quite small in the northern North Atlantic, especially in the region of the subpolar gyre (see Figure 2a in Greatbatch et al., 1991).

Direct wind forcing does, however, influence the PE term, for example, through Ekman pumping, and also, indirectly, the MFA and EMF terms to some extent. To illustrate this, Figure 2 shows the dependence, as obtained from linear regression, of the transport stream function on the winter NAO index. Here the

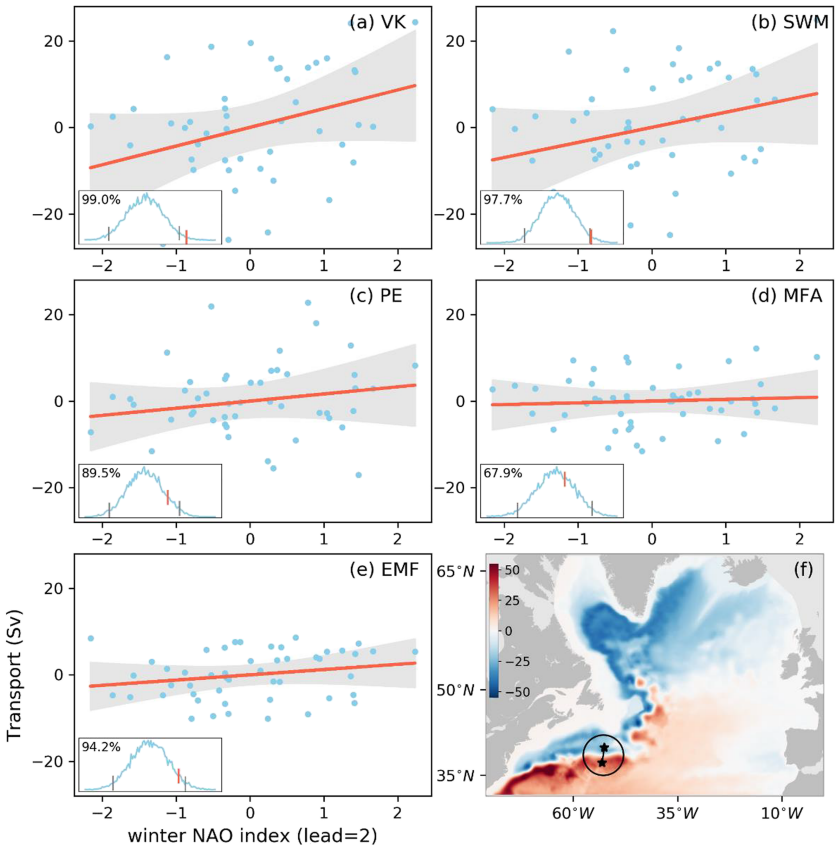

Figure 6. (a–f) As the Figure 4 but for the barotropic transport 2 years later (lead year 2).

transport stream function is a time series of annual means and the winter NAO index is for the months of DJFM, where January, February, and March (JFM) overlap with the year used to compute the annual mean stream function. The WS case is very similar to the response to wind forcing at lag zero noted by Eden and Willebrand (2001) and corresponds to the topographic Sverdrup response to wind forcing. The PE case shows the impact of Ekman pumping, with the tendency to have enhanced gyre transport for both the subpolar and subtropical gyres when the NAO is positive, the latter extending northeastward toward the British Isles. There is also good agreement between VIKING20 and the SWM reconstruction. The feature extending toward the British Isles is enhanced in VIKING20 and the SWM reconstruction compared to the PE case alone through the combination of the contributions from the PE and WS cases. The contributions from the MFA and EMF cases are very localized and do not appear to be important. The WS case will not be discussed further in this paper.

We can also examine how much year-to-year memory is contained in the computed stream functions. Figure 3 shows the time (in years) for the autocorrelation of the stream function to drop to a value of 1/e or less for each case. In order to remove the grid point wave, a centered star-shaped 5-point average is applied in both the zonal and meridional directions to the transport stream function before computing the autocorrelation with a weighting of 1/8 at the outer grid points and 1/2 at the center grid point. In both VIKING20 (Figure 3a) and the SWM reconstruction (Figure 3b), there is memory up to at least 5 years around the northern part of the subpolar gyre. We can see that this memory derives almost entirely from the PE contribution (Figure 3c), that is, the density field. Interestingly, the PE contribution also shows memory extending out to 5 years in the Labrador Sea that is not so evident in either VIKING20 or the SWM reconstruction, indicating how signals in the density field can be obscured by the MFA and EMF contributions. The memory in the PE contribution is consistent with the estimated residence time scale for convectively formed water masses in the Labrador basin (Straneo et al., 2003). The MFA contribution also exhibits some long-term memory in the northern recirculation gyre region south of Atlantic Canada and also around the northern rim of the

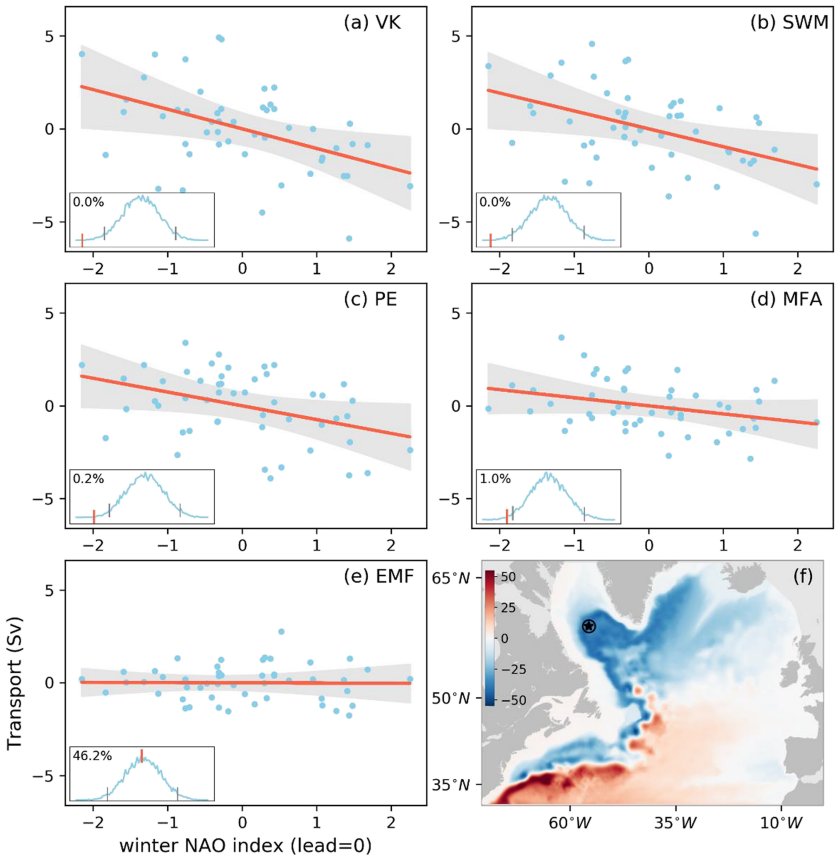

Figure 7. (a–f) As the Figure 4 but for the stream function at the location in the Lavender recirculation shown by the star in panel (f).

Labrador Sea, in the region of the so-called Lavender recirculation (Lavender et al., 2000), although neither of these features appear in VIKING20 or the SWM reconstruction.

We now illustrate how the decomposition technique can be used to understand transport variability associated with the NAO in more detail. In section 1, we noted that the Gulf Stream tends to be further north/south in years following positive/negative NAO winters and although we find some evidence of this in VIKING20 (not shown), the horizontal resolution of the model (1/20 degree, but still only about 5 km in the Gulf Stream region) and the number of years available (50) are such that it is hard to detect movements in Gulf Stream position with any certainty. Instead, we illustrate the transport variability showing, first, the dependence of the transport variability between the two stars shown in Figure 4f. These two stars sit on either side of the Gulf Stream in the model; in particular, one star is in the northern recirculation gyre and the other on the southern flank of the Gulf Stream in the model. As before, the stream function has been filtered to remove grid point waves before applying the analysis and all the analysis uses detrended time series. The light blue dots in Figure 4 show the annual mean transport between the two stars as a function of the winter NAO index along the *x* axis. Here, as before, the winter NAO index is for DJFM and the annual mean is for the year containing JFM (lead year 0). The red straight line is the best fit obtained using linear regression, and the significance of the slope is obtained by randomly shuffling (with no repeats) the annual mean transport amongst the years 10,000 times and repeating the regression analysis. The histogram of the distribution of the regression slopes is presented in the lower left subpanel. The gray bars indicate the 95% significance level for the slope (that is, 2.5% of the total slopes are beyond the gray bar at each end of the histogram), and the slope of the red line is indicated by the red bar. The histogram consists of 100 equally spanned bins from the minimum to the maximum. The percentage of regression slopes from the shuffled samples less than that of the red line is shown: the closer the red line is to the extremes at the two sides of the distribution, the more significant is the dependence shown by the red line. The gray shading shows

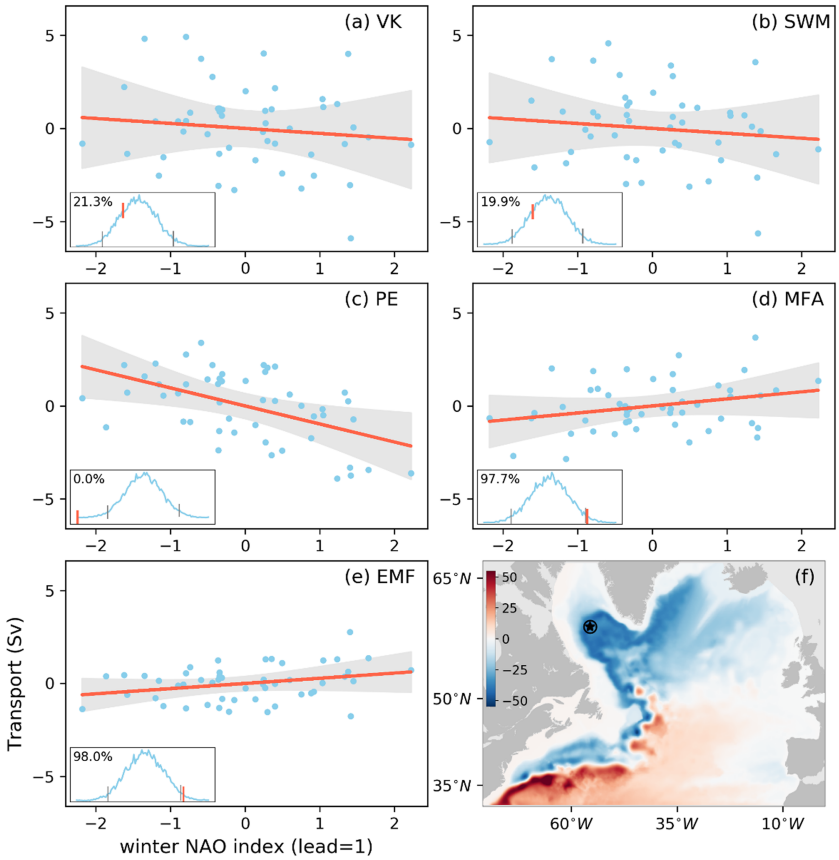

Figure 8. (a–f) As the Figure 7 but for the stream function 1 year later.

the 95% confidence interval of the regressed red line as estimated by randomly resampling the two variables (winter NAO index, x, and transport, y) in pairs, allowing repeated pairs. A distribution of predicted y is obtained by 10,000 regressions on resampled x and y pairs, in this way accounting for noise in both the winter NAO index and the transport.

From Figure 4, we see that in VIKING20, there is a weak tendency at lead year 0 for the transport to increase with increasing NAO index, although this is not statistically significant. This behavior is reproduced by the SWM reconstruction and is a feature of the different contributions to the SWM calculated transport, with the most significant contribution coming from the MFA contribution. In VIKING20, the dependence on the NAO is stronger and more significant 1 year later (lead year 1, Figure 5) and this is also reproduced by the SWM reconstruction. This time, in addition to the MFA contribution, the EMF contribution plays an important role. One year later again (lead year 2, Figure 6), the dependence on the NAO is even stronger in VIKING20 and exceeds the 95% significance threshold, behavior that is again reproduced by the SWM reconstruction. This time, however, it is the EMF contribution that dominates with no significant role for the MFA contribution, but with the PE contribution becoming more important. The results for lead year 3 (not shown) are very similar to those for lead year 2 (Figure 6), and it is only in lead year 4 (not shown) that the significance levels start to drop, with no significant relationship between the NAO and the transport variations in lead year 5 (not shown).

The general features of the results shown in Figures 4–6 are not sensitive to the choice of location either side of the Gulf Stream to compute the transport and show that the variability of the Gulf Stream transport in the recirculation region in the model in response to the winter NAO index is not significant in lead year 0 but is dominated by the MFA and EMF contributions in lead years 1 and 2 (the terms arising from the nonlinear terms in the momentum equations carried by VIKING20). Only in lead year 2, does the baroclinic response (the PE contribution) start to be important and it is the EMF and PE contributions that dominate in lead years 3 and 4. The delayed baroclinic response agrees with the finding of Eden and Willebrand

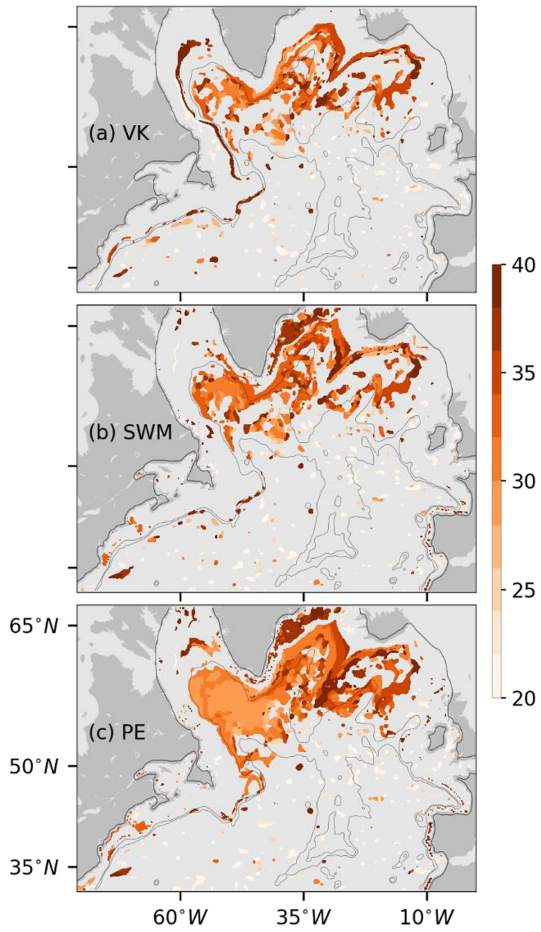

Figure 9. The estimated period (in years) for the internal oscillation implied by the autocorrelation of the transport stream function in (a) VIKING20 (VK), (b) the shallow water model (SWM) reconstruction, and (c) the potential energy (PE) contribution. The period is estimated by doubling the time at which the autocorrelation reaches a minimum that is negative. To be acceptable, the minimum must satisfy two requirements: (1) the minimum autocorrelation must be less than $-1/e$ with a 95% significance level and (2) the autocorrelations must increase at longer lags to become positive with a 95% significance level.

(2001) and is consistent with Gerdes and Köberle (1995), both of whom used non-eddying models. The reason for the relatively rapid response through the MFA and EMF terms is less clear, and constitutes a new result, but suggests that the eddy field may, itself, have some dependence in the NAO. It has been suggested that interannual variability of the eddy kinetic energy in the North Atlantic has a dependence on the NAO (e.g., Stammer & Wunsch, 1999) with a lag of 4 to 12 months (Penduff et al., 2004). Nevertheless, there is no obvious dependence of the eddy kinetic energy on the NAO in VIKING20. There is also no obvious dependence of the MFA and EMF forcing terms used to drive the SWM on the NAO. However, it should be remembered that the transport variability being diagnosed here is an integrated response to the different forcing terms. In the case of the SWM, the zeroth-order description (in the absence of friction) of the model response corresponds to a topographic Sverdrup response to the imposed forcing and is, therefore, an integral along f/H contours in the direction of topographic wave propagation into the basin interior. This process of integration acts to smooth out the noise in the forcing and reveal the signal, in this case the components of transport that are driven by the MFA and EMF terms.

As another example, Figure 7 shows the dependence of the stream function itself at the location shown by the star in Figure 7f within the Lavender recirculation (Lavender et al., 2000) in the northern Labrador Sea. In VIKING20, the stream function shows a significant decreasing dependence on the NAO at lag 0, corresponding to an increase in gyre transport as the NAO index becomes more positive. This behavior is reproduced by the SWM reconstruction and is accounted for by the PE and MFA contributions. It is worth noting that the MFA term is the primary term driving the Lavender gyre in the mean, as noted by Wang et al. (2017). At lead year 1 (Figure 8), the relationship between the NAO and stream function in VIKING20 and the SWM reconstruction becomes less significant, despite a strong contribution from the PE case. The reason for this is that the MFA and EMF contributions, both of which pass the 95% significance threshold, oppose the contribution from the PE case. This is another example of how signals, for example, from the PE terms that are intrinsic to the density field, can be masked by and sometimes even countered by the MFA and EMF contributions.

4. Summary and Discussion

We have shown how the decomposition method introduced by Wang et al. (2017) can be used to analyze the variability of the barotropic stream function and associated transport in a high-resolution model configuration for the northern North Atlantic Ocean, VIKING20 (Behrens, 2013; Böning et al., 2016). The decomposition is based on the vertically averaged momentum equations and is carried out by running a linear SWM to steady state with the forcing terms diagnosed from VIKING20 output. The dominant contribution is from the PE forcing term (which appears as the JEBAR term in the vorticity equation) but with important contributions from the MFA and EMF cases in the Gulf Stream recirculation, North Atlantic Current regions, and the Lavender recirculation. It should be noted that the MFA and EMF arise from the nonlinear advection terms in the momentum equations carried by VIKING20.

The autocorrelation of the transport stream functions demonstrates that the PE contribution, which is intrinsic to the density field, leads to significant memory of the transport stream function in the Labrador Sea and Irminger Sea regions where newly formed waters by deep convection reside. The autocorrelation associated with the PE term remains higher than 1/e for over 5 years in these regions (Figure 3). There is also the suggestion of periodic behavior with a period approaching 30 years (Figure 9). Since this oscillatory

behavior is not found in the NAO index, it seems likely that the oscillatory behavior indicates an internal oceanic mode of variability in the model. Such internal modes of variability in the subpolar gyre region have been suggested by a number of authors, for example, Eden and Greatbatch (2003) and Mecking et al. (2015). The tendency to have oscillatory behavior is also seen in VIKING20 and the SWM but only around the northern rim of the Irminger and Labrador Seas, and not in the interior. This is an example of how transport variability associated with the PE term can be hidden by variability in the MFA and EMF terms arising from the nonlinearity of the momentum equations in VIKING20.

The advantage of the decomposition was also illustrated by looking at how the annual mean barotropic transport in VIKING20 responds to the winter NAO. In particular, we looked at the transport variability in the Gulf Stream recirculation region in VIKING20. Despite there being no significant transport variability associated with the NAO in lead year 0, a tendency for the transport to increase as the winter NAO index increases gradually emerges in lead years 1 and 2 (NAO leading), mostly associated with the MFA and EMF contributions. At lead years 2 and 3, the PE contribution starts to play a role consistent with earlier studies (e.g., Eden & Willebrand, 2001; Marshall et al., 2001) indicating a slow emergence of the baroclinic response to the NAO. It is only in lead year 4 that the response in both VIKING20 and the SWM reconstruction starts to lose significance. The mechanism responsible for the more rapid response associated with the nonlinear (MFA and EMF) terms requires further investigation. Nevertheless, the importance of the MFA and EMF terms in lead years 1 and 2 is a new result.

In the Lavender recirculation (Lavender et al., 2000) in the northern Labrador Sea, both the PE contribution associated with the density field and the MFA advection contribution play an important role in the strong dependence of the transport stream function on the NAO in lead year 0: the more positive the NAO, the stronger the circulation. In the following year (lead year 1), despite a strong contribution from the PE term, the dependence of the stream function on the NAO in both VIKING20 and the SWM reconstruction is much weaker, with the MFA and EMF contributions opposing the dependence from the PE contribution. This again indicates how the nonlinear terms in the momentum equations can obscure transport variability intrinsic to the density field (i.e., the PE contribution) in VIKING20.

Acknowledgments
Yuan Wang is grateful for support from GEOMAR during a 5-month stay during the summer of 2019 when this work was carried out. J. S. is supported by the Natural Sciences and Engineering Research Council of Canada (NSERC), the Ocean Frontier Institute, and MEOPAR. We are grateful to two anonymous reviewers for their helpful comments on the manuscript. The data used in this manuscript can be accessed from http://hdl.handle.net/20.500.12085/4e104bfe-aa9e-4d1e-99fa-5a7d1b9f9313.

References

Anderson, D. L., Bryan, K., Gill, A. E., & Pacanowski, R. C. (1979). The transient response of the North Atlantic: Some model studies. *Journal of Geophysical Research*, *84*(C8), 4795–4815.

Anderson, D. L., & Corry, R. A. (1985). Seasonal transport variations in the Florida Straits: A model study. *Journal of Physical Oceanography*, *15*(6), 773–786.

Anderson, D. L., & Killworth, P. D. (1977). Spin-up of a stratified ocean with topography. *Deep Sea Research*, *24*(8), 709–732.

Behrens, E. (2013). The oceanic response to Greenland melting: The effect of increasing model resolution. Christian-Albrechts-Universität zu Kiel, 8-Diss-136843.

Bell, M. J. (1999). Vortex stretching and bottom torques in the Bryan-Cox ocean circulation model. *Journal of Geophysical Research*, *104*(C10), 23,545–23,563.

Böning, C. W., Behrens, E., Biastoch, A., Getzlaff, K., & Bamber, J. L. (2016). Emerging impact of Greenland meltwater on deepwater formation in the North Atlantic Ocean. *Nature Geoscience*, *9*(7), 523–527.

Breckenfelder, T., Rhein, M., Roessler, A., Böning, C. W., Biastoch, A., Behrens, E., & Mertens, C. (2017). Flow paths and variability of the North Atlantic Current: A comparison of observations and a high-resolution model. *Journal of Geophysical Research: Oceans*, *122*, 2686–2708. https://doi.org/10.1002/2016JC012444

Curry, R. G., & McCartney, M. S. (2001). Ocean gyre circulation changes associated with the North Atlantic Oscillation. *Journal of Physical Oceanography*, *31*(12), 3374–3400.

De Coëtlogon, G., Frankignoul, C., Bentsen, M., Delon, C., Haak, H., Masina, S., & Pardaens, A. (2006). Gulf Stream variability in five oceanic general circulation models. *Journal of Physical Oceanography*, *36*(11), 2119–2135.

Delworth, T., Manabe, S., & Stouffer, R. J. (1993). Interdecadal variations of the thermohaline circulation in a coupled ocean-atmosphere model. *Journal of Climate*, *6*(11), 1993–2011.

Dickson, R., Lazier, J., Meincke, J., Rhines, P., & Swift, J. (1996). Long-term coordinated changes in the convective activity of the North Atlantic. *Progress in Oceanography*, *38*(3), 241–295.

DiNezio, P. N., Gramer, L. J., Johns, W. E., Meinen, C. S., & Baringer, M. O. (2009). Observed interannual variability of the Florida Current: Wind forcing and the North Atlantic Oscillation. *Journal of Physical Oceanography*, *39*(3), 721–736.

Drews, A., Greatbatch, R. J., Ding, H., Latif, M., & Park, W. (2015). The use of a flow field correction technique for alleviating the North Atlantic cold bias with application to the Kiel climate model. *Ocean Dynamics*, *65*(8), 1079–1093.

Eden, C., & Greatbatch, R. J. (2003). A damped decadal oscillation in the North Atlantic Climate System. *Journal of Climate*, *16*(24), 4043–4060.

Eden, C., & Jung, T. (2001). North Atlantic interdecadal variability: Oceanic response to the North Atlantic Oscillation (1865–1997). *Journal of Climate*, *14*(5), 676–691.

Eden, C., & Willebrand, J. (2001). Mechanism of interannual to decadal variability of the North Atlantic circulation. *Journal of Climate*, *14*, 2266–2280.

Gerdes, R., & Köberle, C. (1995). On the influence of DSOW in a numerical model of the North Atlantic general circulation. *Journal of Physical Oceanography*, *25*(11), 2624–2642.
Greatbatch, R. J. (2000). The North Atlantic Oscillation. *Stochastic Environmental Research and Risk Assessment*, *14*(4–5), 213–242.
Greatbatch, R. J., Fanning, A. F., Goulding, A. D., & Levitus, S. (1991). A diagnosis of interpentadal circulation changes in the North Atlantic. *Journal of Geophysical Research*, *96*(C12), 22,009–22,023.
Greatbatch, R. J., Zhai, X., Claus, M., Czeschel, L., & Rath, W. (2010). Transport driven by eddy momentum fluxes in the Gulf Stream Extension region. *Geophysical Research Letters*, *37*, L244001. https://doi.org/10.1029/2010GL045473
Hurrell, J. W. (1995). Decadal trends in the North Atlantic Oscillation: Regional temperatures and precipitation. *Science-AAAS-Weekly Paper Edition*, *269*(5224), 676–678.
Hurrell, J. W., Kushnir, Y., Ottersen, G., & Visbeck, M. (2003). An overview of the North Atlantic Oscillation. *Geophysical Monograph Series*, *134*, 1–35.
Joyce, T. M., Deser, C., & Spall, M. A. (2000). The relation between decadal variability of subtropical mode water and the North Atlantic Oscillation. *Journal of Climate*, *13*(14), 2550–2569.
Joyce, T. M., & Zhang, R. (2010). On the path of the Gulf Stream and the Atlantic Meridional Overturning Circulation. *Journal of Climate*, *23*(11), 3146–3154.
Large, W. G., & Yeager, S. G. (2009). The global climatology of an interannually varying air–sea flux data set. *Climate Dynamics*, *33*(2–3), 341–364.
Lavender, K. L., Davis, R. E., & Owens, W. B. (2000). Mid-depth recirculation observed in the interior Labrador and Irminger seas by direct velocity measurements. *Nature*, *407*(6800), 66–69. https://doi.org/10.1038/35024048
Lazier, J. R. N. (1994). Observations in the northwest corner of the North Atlantic Current. *Journal of Physical Oceanography*, *24*(7), 1449–1463.
Madec, G. (2008). NEMO reference manual, ocean dynamic component: NEMO-OPA. Note Du Pôle de Modélisation, Institut Pierre Simon Laplace, France, Technical Report, *27*.
Marshall, J., Johnson, H., & Goodman, J. (2001). A study o f the interaction of the North Atlantic Oscillation with ocean circulation. *Journal of Climate*, *14*(7), 1399–1421.
McCarthy, G. D., Joyce, T. M., & Josey, S. A. (2018). Gulf Stream variability in the context of quasi-decadal and multidecadal Atlantic climate variability. *Geophysical Research Letters*, *45*, 11,257–11,264. https://doi.org/10.1029/2018GL079336
Mecking, J. V., Keenlyside, N. S., & Greatbatch, R. J. (2015). Multiple time scales of stochastically forced North Atlantic Ocean variability: A model study. *Ocean Dynamics*, *65*, 1367–1381.
Mellor, G. L., Mechoso, C. R., & Keto, E. (1982). A diagnostic calculation of the general circulation of the Atlantic Ocean. *Deep Sea Research Part A. Oceanographic Research Papers*, *29*(10), 1171–1192.
Mertz, G., & Wright, D. G. (1992). Interpretations of the JEBAR term. *Journal of Physical Oceanography*, *22*(3), 301–305.
Penduff, T., Barnier, B., Dewar, W. K., & O'Brien, J. J. (2004). Dynamical response of the oceanic eddy field to the North Atlantic Oscillation: A model–data comparison. *Journal of Physical Oceanography*, *34*(12), 2615–2629.
Rieck, J. K., Böning, C. W., Greatbatch, R. J., & Scheinert, M. (2015). Seasonal variability of eddy kinetic energy in a global high-resolution ocean model. *Geophysical Research Letters*, *42*, 9379–9386. https://doi.org/10.1002/2015GL066152
Rossby, T., Flagg, C., & Donohue, K. (2010). On the variability of Gulf Stream transport from seasonal to decadal timescales. *Journal of Marine Research*, *68*(3), 503–522.
Smeed, D. A., Josey, S. A., Beaulieu, C., Johns, W. E., Moat, B. I., Frajka-Williams, E., et al. (2018). The North Atlantic Ocean is in a state of reduced overturning. *Geophysical Research Letters*, *45*, 1527–1533. https://doi.org/10.1002/2017GL076350
Stammer, D., & Wunsch, C. (1999). Temporal changes in eddy energy of the oceans. *Deep Sea Research Part II: Topical Studies in Oceanography*, *46*(1–2), 77–108.
Straneo, F., Pickart, R. S., & Lavender, K. (2003). Spreading of Labrador sea water: An advective-diffusive study based on Lagrangian data. *Deep-Sea Research Part I: Oceanographic Research Papers*, *50*(6), 701–719.
Taylor, A. H., & Stephens, J. A. (1998). The North Atlantic Oscillation and the latitude of the Gulf Stream. *Tellus A*, 134–142.
Wang, Y., Claus, M., Greatbatch, R. J., & Sheng, J. (2017). Decomposition of the mean barotropic transport in a high-resolution model of the North Atlantic Ocean. *Geophysical Research Letters*, *44*, 11,537–11,546. https://doi.org/10.1002/2017GL074825
Watelet, S., Beckers, J. M., & Barth, A. (2017). Reconstruction of the Gulf Stream from 1940 to the Present and correlation with the North Atlantic Oscillation. *Journal of Physical Oceanography*, *47*(11), 2741–2754.
Yashayaev, I. (2007). Hydrographic changes in the Labrador Sea, 1960–2005. *Progress in Oceanography*, *73*(3–4), 242–276.
Yeager, S. (2015). Topographic coupling of the Atlantic overturning and gyre circulations. *Journal of Physical Oceanography*, *45*(5), 1258–1284.